ent gate voltages. As long as V_{DS} is low and does not reach pinchoff, the negative transconductance feature appears. At higher V_{DS}, the gate electric field becomes position dependent along the channel, which smears out the resonant coupling effect and its consequences. This leads to the crossing of I_{DS}-V_{DS} curves. In the saturation region, the drain current I_{DSsat} is mostly determined by the total number of electrons in the channel, resulting in the usual FET characteristics.

Fig. 2 indicates that this FET should function as n-channel or p-channel-like device and also as a frequency multiplier, as long as the gate voltage is properly modulated. Fig. 4*b* shows one such example of a resistor-loaded circuit, which multiplies the frequency of the gate input by a factor of 3, as shown in Fig. 4*a*.

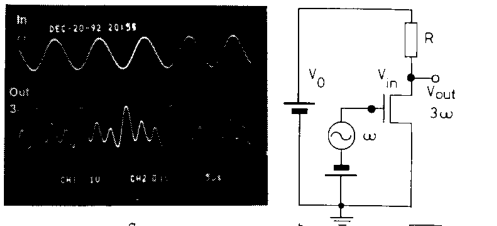

Fig. 4 *Oscilloscope traces of input voltage $V_{in} = -0{\cdot}3\,V + 0{\cdot}7\,V \sin \omega t$, and output voltage of resistor-loaded circuit, where resistance is set at $1\,k\Omega$ and $V_0 = 1\,V$*

a Input voltage
b Output voltage
Parameters are set to multiply the input frequency by 3.

In summary, we have demonstrated novel features in a double quantum well field-effect transistor and have shown its desirable device functions and also excellent compatibility with normal FETs in operation and fabrication process.

Acknowledgments: Y. Ohno acknowledges the stimulating discussion with T. Noda and T. Matsusue. This work is partly supported by a grant-in-aid from the Ministry of Education, Science and Culture, Japan.

11th January 1993

Y. Ohno (*Institute of Industrial Science, University of Tokyo, 7-22-1 Roppongi, Minsyo-ku, Tokyo 106, Japan, and Research Center for Advanced Science and Technology, University of Tokyo, 4-6-1 Komaba, Meguro-ku, Tokyo 106, Japan*)

M. Tsuchiya (*Department of Information and Communication Engineering, University of Tokyo, 7-3-1 Hongo, Bunkyo-ku, Tokyo 113, Japan*)

H. Sakaki (*Institute of Industrial Science, University of Tokyo, 7-22-1 Roppongi, Minato-ku, Tokyo 106, Japan, Research Center for Advanced Science and Technology, University of Tokyo, 4-6-1 Komaba, Meguro-ku, Tokyo 106, Japan, and Quantum Wave Project, JRDC, 4-3-24-302 Komaba, Meguro-ku, Tokyo 153, Japan*)

References

1 CHANG, L. L., ESAKI, L., and TSU, R.: 'Resonant tunneling in semiconductor double barriers', *Appl. Phys. Lett.*, 1974, **24**, pp. 593–595
2 YOKOYAMA, N., IMAMURA, K., MUTO, S., HIYAMIZU, S., and NISHI, H.: 'A new functional, resonant-tunneling hot electron transistor (RHET)', *Jpn. J. Appl. Phys.*, 1985, **24**, pp. L853–L854
3 YANG, C. H., KAO, Y. C., and SHIH, H. D.: 'New field-effect resonant tunneling transistor: Observation of oscillatory transconductance', *Appl. Phys. Lett.*, 1989, **55**, pp. 2742–2744
4 SAKAKI, H.: 'Velocity-modulation transistor (VMT)-A new field-effect transistor concept', *Jpn. J. Appl. Phys.*, 1982, **21**, pp. L381–383
5 VINTER, B., and TARDELLA, A.: 'Tunneling transfer field-effect transistor: A negative transconductance device', *Appl. Phys. Lett.*, 1987, **50**, pp. 410–412
6 PALEVSKI, A., BELTRAM, F., CAPASSO, F., PFEIFFER, L., and WEST, K. W.: 'Resistance resonance in coupled potential wells', *Phys. Rev. Lett.*, 1990, **65**, pp. 1929–1932

NOVEL DIGITAL INTEGRATOR AND DIFFERENTIATOR

M. A. Al-Alaoui

Indexing terms: Digital circuits, Circuit design, Integrated circuits

A novel digital integrator and a novel digital differentiator are presented. Both the integrator and the differentiator are of first order and thus eminently suitable for real-time applications. Both have an almost linear phase. The integrator is obtained by interpolationg two popular digital integration techniques, the rectangular and the trapezoidal rules. The resulting integrator outperforms both the rectangular and the trapezoidal integrators in range and accuracy. The new differentiator is obtained by taking the inverse of the transfer function of the integrator. The effective range of the differentiator is about 0·8 of the Nyquist frequency.

Basic concept: The basic concept came from observing that the ideal integrator response lies between the responses of the rectangular rule and the trapezoidal rule [1]. Thus it seems reasonable that interpolating the above two rules would result in a new integrator that could better approximate the ideal integrator.

New nonminimum phase digital integrator: It can be seen from Fig. 1 that the magnitude of the frequency response of the ideal integrator falls between the magnitudes of the rectangular and the trapezoidal integrators. This suggests approximating the ideal integrator as a weighted sum of the rectangular and the trapezoidal integrators. At half the Nyquist frequency the ratio is $\sim 1:3$. Reflecting this observation to the transfer functions, the following relation between the transfer functions of the integrators is obtained. The subscript N denotes the new integrator, R denotes the rectangular integrator, and T denotes the trapezoidal integrator:

$$H_N(z) = \tfrac{3}{4}H_R(z) + \tfrac{1}{4}H_T(z) \tag{1}$$

Substituting the corresponding transfer functions in eqn. 1, we obtain

$$H_N(z) = \left(\frac{3}{4}\right)\frac{T}{(z-1)} + \left(\frac{1}{4}\right)\frac{T(z+1)}{2(z-1)} \tag{2}$$

Simplifying eqn. 2, we obtain the following transfer function of the new integrator:

$$H_N(z) = \left(\frac{T}{8}\right)\frac{(z+7)}{(z-1)} \tag{3}$$

Note that $T = 1$ in the frequency plots shown in Fig. 1, and

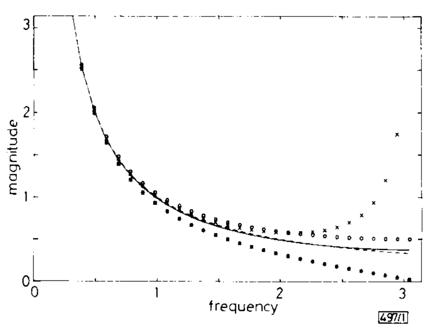

Fig. 1 *Magnitude response of new integrator, and ideal, trapezoidal, and rectangular integrators, and Simpson integrators*

——— new
- - - - ideal
○ trapezoidal
∗ rectangular
× Simpson

the Nyquist frequency is π. However in Figs. 2–6, the Nyquist frequency is normalised to 1. All the Figures in this Letter were obtained by using MATLAB* together with the Signal Processing Toolbox.*

Fig. 2 shows the percent relative magnitude error of the new integrator compared with the magnitude response of the ideal integrator. Fig. 3 shows the phase of the new integrator which is almost linear with a maximum phase error of 8·25° occurring at 0·55 of the Nyquist frequency. The ideal linear phase, shown as a dotted line, corresponds to an ideal integrator with half a sample of delay.

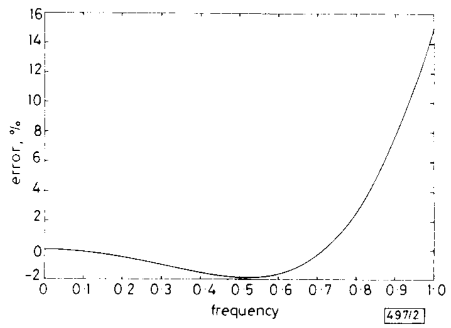

Fig. 2 *Percent relative error of magnitude response of new integrator and new differentiator*

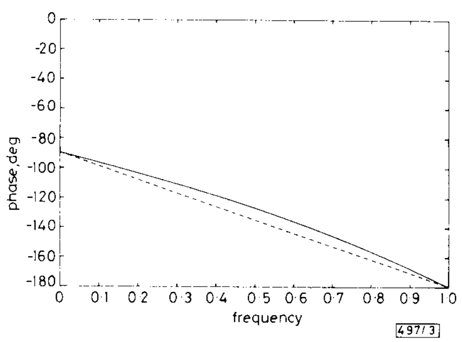

Fig. 3 *Phase response of nonminimum phase integrator and corresponding linear phase integrator*

——— nonminimum phase integrator
– – – – linear phase integrator

New minimum phase digital integrator: To obtain a minimum phase digital integrator, reflect the zero at $z = -7$ to a zero at $z = -1/7$ and compensate for the magnitude appropriately by multiplying the resulting minimum phase transfer function by r [2]. Thus the resulting transfer function of the minimum phase integrator is

$$H(z) = 7\,\frac{T}{8}\,\frac{(z + \frac{1}{7})}{(z - 1)} \tag{4}$$

The magnitude response is the same as that of the nonminimum phase integrator. The phase response of the minimum phase integrator is shown in Fig. 4.

New digital differentiator: In this Letter the proposed new differentiator is obtained by inverting the transfer function of the minimum phase integrator developed in the preceding Section [3].

The resulting transfer function of the new digital differentiator is

$$G(z) = \frac{8(z - 1)}{7T(z + \frac{1}{7})} \tag{5}$$

* Trademark of The Mathworks Inc.

Fig. 5 shows the magnitude response of the new differentiator which approximates the ideal differentiator, shown as a dotted line, up to 0·78 of the Nyquist frequency within a 2% error. This compares favourably with the 5 point differentiator reported by Oppenheim and Schafer [4]. The percent relative magnitude error is the same as that of the new integrator shown in Fig. 2. Fig. 6 shows the phase response of the new

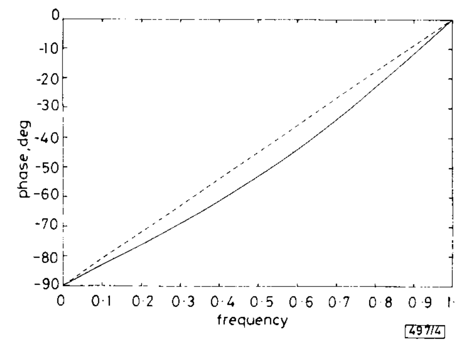

Fig. 4 *Phase response of minimum phase integrator and corresponding linear phase integrator*

——— minimum phase integrator
– – – – linear phase integrator

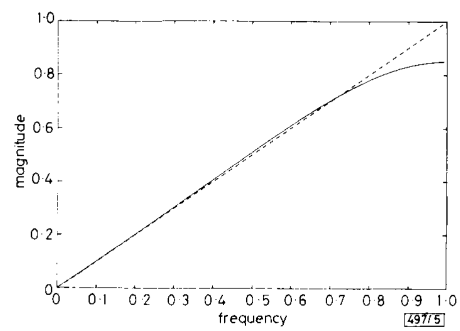

Fig. 5 *Magnitude response of new differentiator and ideal differentiator*

——— new differentiator
– – – – ideal differentiator

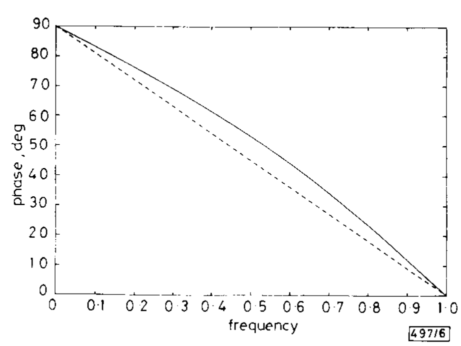

Fig. 6 *Phase response of new differentiator and corresponding linear phase differentiator*

——— new differentiator
– – – – linear phase differentiator

differentiator which approximates the linear phase, shown as a dotted line, of the ideal differentiator with half a sample of delay. The maximum error is 8·25° occurring at 0·55 of the Nyquist frequency. This is better than the 10·5° occurring at 0·6 of the Nyquist frequency reported by Rabiner and Steiglitz [5] using higher order recursive differentiators. A midband frequency differentiator could be obtained by realising the pole at say $z = 0{\cdot}99, \ldots$, instead of at $z = 1$. The resulting differentiators compare favourably with the state of the art differentiators of Kumar and Dutta-Roy [6].

Acknowledgment: It is a pleasure to thank T. Kailath for providing the atmosphere conducive to research by inviting me to spend the summer of 1991 at Stanford's Information Systems Lab. where this research was initiatied. I am also grateful to B. McKee, M. Goldburg, D. Roy, L. Tong, N. Al-Dhahir, Guanghan Xu, H. Aghajan, A. Sayed and C. Schaper for their help during my stay at Stanford. This work was supported in part by the Research Board of The American University of Beirut.

4th January 1993

M. A. Al-Alaoui (*Electrical Engineering Department, The American University of Beirut, Beirut, Lebanon*)

References

1 TOMPKINS, W. J., and WEBSTER, J. G. (Eds.): 'Design of microcomputer-based medical instrumentation' (Prentice-Hall, Englewood Cliffs, NJ, 1981)

2 STEIGLITZ, K.: 'Computer-aided design of recursive digital filters', *IEEE Trans.*, 1970, **AU-18**, pp. 123–129

3 AL-ALAOUI, M. A.: 'Novel approach to designing digital differentiators', *Electron. Lett.*, 1992, **28**, (15), pp. 1376–1378

4 OPPENHEIM, A. V., and SCHAFER, R. W.: 'Discrete-time signal processing' (Prentice-Hall, Englewood Cliffs, NJ, 1989)

5 RABINER, L. R., and STEIGLITZ, K.: 'The design of wide-band recursive and nonrecursive digital differentiators', *IEEE Trans.*, 1970, **AU-18**, pp. 204–209

6 KUMAR, B., and DUTTA-ROY, S. C.: 'Design of efficient FIR digital differentiators and Hilbert transformers for midband frequency ranges', *Int. J. Circuit Theory Appl.*, 1989, **17**, (4), pp. 483–488

NOVEL POLARIMETRIC FIBRE DEVICE FOR INTERROGATING 'WHITE-LIGHT' INTERFEROMETERS

M. G. Xu, M. Johnson, M. Farhadiroushan and J. P. Dakin

Indexing terms: Optical sensors, Polarisation, Optical fibres

A novel, in-line, polarimetric fibre interrogator for 'white-light' interferometry is described. It consists of two equal lengths of polarisation-maintaining fibre, spliced with their polarisation axes orthogonal. The interferometer path difference is thermally tuned over the free-space equivalent of $\pm 180\,\mu m$ to allow matching to a remote sensor interferometer.

Introduction: 'White-light' interferometry (WLI) has, over the past few years, become an important fibre sensing technique [1–3]. It provides a means of identifying both the absolute optical interference fringe order and the residual phase angle in a remote, unbalanced interferometer. In a typical system, a broadband source is coupled through a remote sensing interferometer, such as a Fabry–Perot, with an optical path difference (OPD) d. This acts as an optical filter which imparts a periodic modulation on the initially smooth spectrum, the pitch of which characterises the OPD of the sensor. In a time-domain description of the effect, light beams proagating via the two paths of the interferometer are only correlated if the light in the shorter path is subsequently delayed by a time $2d/v_g$, where v_g is the group velocity in the interferometer. If a value of d is chosen which is significantly larger than the correlation length of the broadband source, then, without such a compensating delay, small variations in d will not cause visible interference fringes in the integrated signal.

If, however, the optical signal is then passed through a second interferometer, whose path imbalance can be scanned, then high-visibility interference fringes will be detected when the *magnitude* of the path difference closely matches that in the remote interferometer. An independent measurement of the local delay thus allows determination of the magnitude of the unknown remote delay, free from ambiguities. The technique can give high accuracy, but it generally requires moving parts in the readout interferometer (e.g. the scanned Michelson [1]) or involves a relatively complex optical spectrometer arrangement (e.g. a dispersive element plus CCD detector).

We present a new method of constructing a thermally-scanned polarimetric interferometer, using two, nominally-equal, lengths of polarisation-maintaining (PM) fibre, spliced together with their polarisation axes at 90°. The arrangement is essentially that of the compensated polarimetric interferometer which has been used for differential sensing [4]. If not mechanically strained, the OPD between the two polarisation modes in the polarimetric interferometer depends primarily on the temperature difference $\Delta T = T_1 - T_2$ between the two fibre lengths. By scanning the temperature difference, a controllable differential mode delay can be generated, for matching the OPD of the remote interferometer. The advantages of this technique over other methods are that the readout interferometer is a single length of fibre, without any moving parts, and the whole system may be spliced into an optically efficient and compact unit. In addition, operation is possible in wavelength regions where detector arrays are less readily available, and the single small-area detector possible with this technique offers lower noise than with self-scanned arrays.

Experiment: Fig. 1 depicts the thermally-scanned, in-line, fibre WLI interrogation system. Light from a 1550 nm fibre-pigtailed ELED, of $1/e^2$ bandwidth ± 42 nm, is coupled, via a

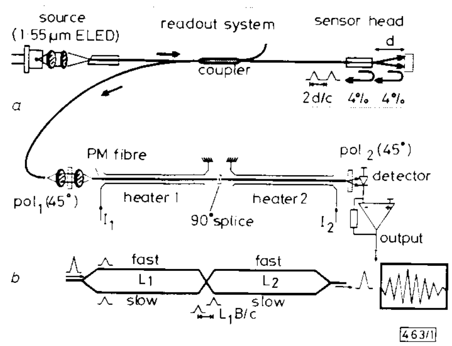

Fig. 1 *Schematic diagram of thermally-scanned in-line fibre white-light matched interferometry, and illustration of fast and slow propagation paths in 90°-spliced fibre lengths*

a Schematic diagram
b Illustration of fast and slow propagation paths

directional fibre coupler into a Fabry–Perot interferometer, having a separation d, to simulate a remote sensor. The power level at the sensor was $4\,\mu W$. The Fabry–Perot cavity was formed between the end face of a singlemode fibre and a reflective glass block mounted on a positioner. The rear surface of the block was rough-ground and painted to avoid spurious reflections. The low Fresnel reflectivity at each surface ($<4\%$) meant that the Fabry–Perot effectively acted as a low finesse, two-beam (rather than multiple-beam) interferometer. The effective delay time of the sensor head was therefore $2d/c$, where c is the velocity of light.

The receiving polarimetric interferometer was formed from two lengths ($L_1 = 10097$ mm, $L_2 = 10073$ mm) of PM fibre (York Ltd. HB1550) with beatlength 3·06 mm. In our case, L_1 and L_2 were first matched to within $24 \pm 0{\cdot}5$ mm, giving a mismatch of only seven fringes when the fibres are of equal temperatures. Initial matching was carried out using a commercial York S18 chromatic dispersion instrument. Subsequent shortening of one fibre reduced the mismatch to less than one fringe. Equal optical power was launched into the fast and slow eigenaxes, i.e. there were equal intensity beams travelling in the fast and slow states. At the central splice, fast and slow axes are interchanged, so that for equal lengths and temperatures ($L_1 = L_2$, $T_1 = T_2$) the differential delay is zero. Each length of PM fibre was contained within separate stain-